Supplementary Material for
Supersonic screw dislocations gliding at the shear wave speed

Shenyou Peng[1,4], Yujie Wei[1,4*], Zhaohui Jin[2], Wei Yang[3]

[1]LNM, Institute of Mechanics, Chinese Academy of Sciences, Beijing 100190, China
[2]Light Alloy Net Forming National Engineering Research Center & School of Materials Science and Engineering, Shanghai Jiao Tong University, Shanghai 200240, China
[3]Institute of Applied Mechanics and Center for X-Mechanics, Zhejiang University, Hangzhou 310027, China
[4]School of Engineering Sciences, University of Chinese Academy of Sciences, Beijing 100049, China

*To whom correspondence should be addressed: yujie_wei@Lnm.imech.ac.cn (Y. Wei)

Note 1: Modelling details

We simulate the motion of screw dislocation using the large-scale atomic/molecular massively parallel simulator (LAMMPS) [1]. The embedded atom method (EAM) potential for copper is used herein [2]. Periodic boundary condition is chosen in all three dimensions. To proceed, we use a screw dislocation dipole to maintain a zero-sum Burgers vector, which is realized by displacing the upper block by $b/2$ and bottom block by $-b/2$, where b is the unit Burgers vector of the perfect screw dislocation, as shown in Fig. 1a.

Three dimensions of the sample are $L_x = 1328\text{nm}$, $L_y = 250\text{nm}$, and $L_z = 0.767\text{nm}$. The (x, y) coordinates of the two screw dislocations (SD) of opposite sign are about (665nm, 62nm) and (665nm, 188nm), respectively. As for quadruple twinning screw partial dislocation (TSPD), the coordinates are about (442nm, 62nm), (442nm, 188nm), (884nm, 62nm) and (884nm, 188nm) respectively. Fig. S1 demonstrate the atomic structures of the SD and TSPD. Sufficiently large simulation box is desired in order to eliminate possible size effect caused by interactions among the periodic arrangement of dislocations or image stress due to surface effect in finite

samples. Before straining, the initial system will be relaxed for 10ps to a stress-free state. We subsequently apply loading to monitor the motion of screw dislocation. To resemble the experimental loadings, two loading sequences will be employed, namely strain loading (at strain rate of $5 \times 10^8/\mathrm{s}$) and stress loading. All simulations are performed at a constant temperature of T=1K. Unless stated otherwise, atoms in the dislocation core (e.g., those shown in Fig. 2d) is traced by the Common Neighbor Analysis (CNA) [3].

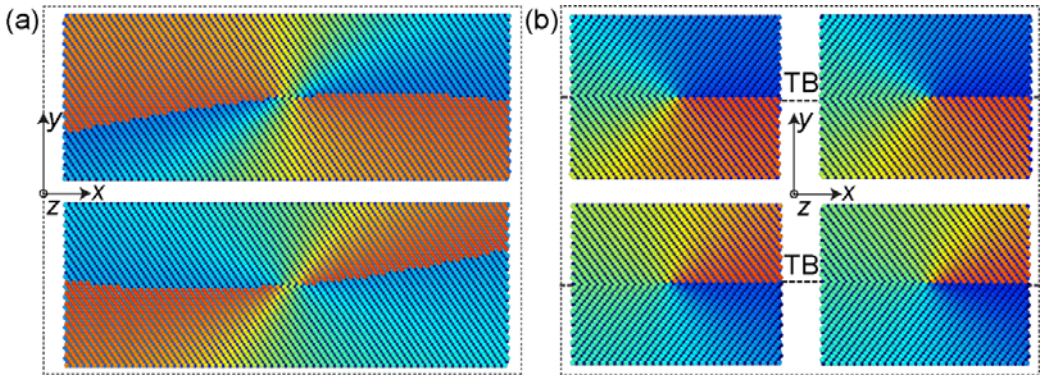

Figure S1. Atomic structures of perfect screw dislocations (SDs) and twinning screw partial dislocations (TSPDs). (a) A SD dipole under periodic boundary conditions. (b) A quadruple configuration formed by four TSPDs residing in a twin boundary. Atoms are colored by their z-coordinates.

Note 2: Dissociation of screw dislocations

A perfect screw dislocation in F.C.C crystal will split into two Shockley partials with a stacking fault in between, following the dislocation reaction $\frac{a}{2}[1\bar{1}0] = \frac{a}{6}[1\bar{2}1] + \frac{a}{6}[2\bar{1}\bar{1}] + \mathrm{SF}$. Fig. S2a sketches the dissociation of a full screw dislocation $\vec{b} = \frac{a}{2}[1\bar{1}0]$ into two partials $\vec{b}_1 = \frac{a}{6}[1\bar{2}1]$ and $\vec{b}_2 = \frac{a}{6}[2\bar{1}\bar{1}]$, and each is composed of an edge component $\vec{b}_{ei}$ and a screw part $\vec{b}_{si}$ $(i = 1,2)$, and their respective magnitudes are $b_s = |\vec{b}_{si}| = b/2$ and $b_e = |\vec{b}_{ei}| = b/2\sqrt{3}$. Here b is the magnitude of the Burgers

vector $\vec{b}$. Using the Peierls–Nabarro model [4], the displacement mismatch between the neighboring intact layer and the dislocated layer is described by

$$u_z = \frac{b_s}{\pi}\left(\arctan\frac{x-d/2}{w} + \arctan\frac{x+d/2}{w}\right) \quad \text{(S1a)}$$

for the screw part and

$$u_x = \frac{b_e}{\pi}\left(-\arctan\frac{x-d/2}{w} + \arctan\frac{x+d/2}{w}\right) \quad \text{(S1b)}$$

for the edge part, where d is the stacking fault width given as [5]

$$d = \frac{G\left|\vec{b}_i\right|^2}{8\pi E_{sf}}\frac{2-3\nu}{1-\nu} \quad \text{(S2)}$$

and G denotes the shear modulus, E_{sf} the intrinsic stacking fault energy, and ν is the Poisson's ratio. The characteristic dislocation core width w is defined as $w = \frac{a}{2(1-\nu)}$. For Cu, we have $G = 46\ \mathrm{GPa}$, $E_{sf} = 44\ \mathrm{mJ/m^2}$, $\nu = 0.34$ and $a = 3.615\ \text{Å}$.

Noting that the Burgers vector of the TSPD is the same as the dissociated SD, i.e. $\vec{b}_1 = \frac{a}{6}[1\bar{2}1]$ and $\vec{b}_2 = \frac{a}{6}[2\bar{1}\bar{1}]$, but stacking fault free. The displacement mismatch analysis is consistent with eqn. (S1) when d is arbitrary. Using a normalized displacement shift ϕ with $\phi = u/b$, we show in Figs. 1b and 1c characterize the core structure of the dissociated SD and the TSPD, the MD simulations (circles) agree well with theoretical prediction (solid line). The dislocation core can also be featured by the misfit density $\mathrm{d}\phi/\mathrm{d}x$, as Fig. S2 shows. For the dissociated SD, the separation of partials d is the distance between the cores of two partial; For the TSPD, we show one characteristic partials only.

Further detailed atomistic information of both the SD and TSPD is furnished in Fig. S3, with Fig. S3a for the atomic structure of the separated SD and S3b for the twinning partial, respectively.

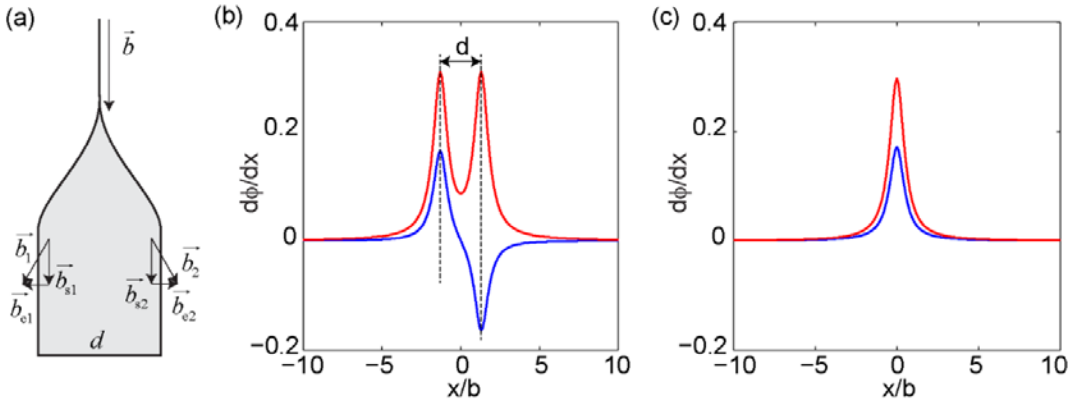

Figure S2. Core structure of the SD and TSPD. (a) Dissociation of a SD into two partials. Each partial is of a mixed character, composed of a pure edge part and a pure screw part; (b) and (c) misfit density of the SD and TSPD, respectively.

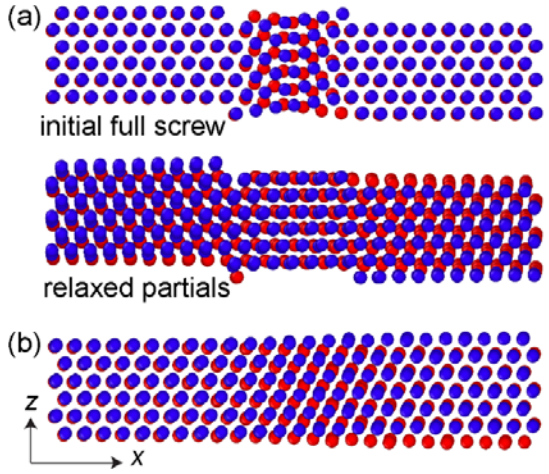

Figure S3. The atomic position of the neighboring layers across the shear plane of screw dislocations in FCC Cu. (a) Atomic structures to show the decomposition of a perfect SD into two partials after relaxation. (b) The atomic structure of a TSPD.

Note 3: Stress field of screw dislocations

We adopted the classical anisotropic elasticity theory of straight dislocations [6]. The continuum equations of stresses introduced by a screw dislocation in the face-centered cubic (F.C.C.) crystals are obtained as follows. F.C.C. copper has three independent elastic constants C_{11}, C_{12}, C_{44} in the 6×6 symmetric stiffness tensor $\boldsymbol{C}$ in the conventional coordinate system defined by $X = [100], Y = [010], Z = [001]$. A rectangular coordinate defined by $x = [11\bar{2}], y = [111], z = [1\bar{1}0]$ in accordance with

the screw dislocation is desired. The components Q_{klmn} in the fourth-rank transformation matrix $\boldsymbol{Q}$ is given as $Q_{klmn} = T_{km}T_{ln}$, with $T_{ij} = \cos(X_i, x_j)$ and i, j, k, l, m, n=1,2,3. The elastic stiffness $\boldsymbol{C}'$ in the (x, y, z) coordinate is related to $\boldsymbol{C}$ in (X, Y, Z) by $\boldsymbol{C}' = \boldsymbol{Q} \cdot \boldsymbol{C} \cdot \boldsymbol{Q}$. Now the stress induced by edge part b_e is [5]:

$$\sigma_{ij} = -\frac{M}{\rho^4}\frac{b_e}{2\pi}\left\{C'_{ij11}\left[(\bar{C}_{11} + C'_{12} + C'_{66})x^2y + \frac{\bar{C}_{11}}{C'_{22}}y^3\right] - C'_{ij12}(\bar{C}_{11} + C'_{12})\left(x^3 - \frac{\bar{C}_{11}}{C'_{22}}xy^2\right) - \frac{C'_{ij22}}{C'_{22}}\left[(C'^2_{12} + \bar{C}_{11}C'_{12} + 2\bar{C}_{11}C'_{66} + \bar{C}_{11}C'_{66})x^2y - \frac{\bar{C}^2_{11}C'_{66}}{C'_{22}}y^3\right]\right\}, \quad \text{(S3)}$$

with

$\bar{C}_{11} = (C'_{11}C'_{22})^{1/2}$, $M = \left[\frac{\bar{C}_{11} - C'_{12}}{C'_{22}C'_{66}(\bar{C}_{11} + C'_{12} + 2C'_{66})}\right]^{1/2}$,

and $\rho^4 = \left(x^2 + \frac{\bar{C}_{11}}{C'_{22}}y^2\right)^2 + \frac{(\bar{C}_{11} + C'_{12})(\bar{C}_{11} - C'_{12} - 2C'_{66})}{C'_{22}C'_{66}}x^2y^2$,

where $\boldsymbol{C}'$ is the transformed elastic stiffness.

For the screw part b_s, the non-zero stress components are given as [5]:

$$\begin{aligned}\sigma_{yz} &= -\frac{b_s}{2\pi}\left(C'_{44}C'_{55} - C'^2_{45}\right)^{\frac{1}{2}}\frac{C'_{44}x - C'_{45}y}{C'_{44}x^2 - 2C'_{45}xy + C'_{55}y^2},\\ \sigma_{xz} &= -\frac{b_s}{2\pi}\left(C'_{44}C'_{55} - C'^2_{45}\right)^{\frac{1}{2}}\frac{C'_{45}x - C'_{55}y}{C'_{44}x^2 - 2C'_{45}xy + C'_{55}y^2},\end{aligned} \quad \text{(S4)}$$

where $C'_{44}, C'_{45}, C'_{55}$ are the corresponding components in $\boldsymbol{C}'$.

Note 4: Shear wave

Given the anisotropic elasticity in single crystals, shear wave speeds are intrinsically anisotropic in F.C.C. Cu. Using a coordinate system with its axes parallel to the cube axes, $X = [100], Y = [010], Z = [001]$, one may write the elastic wave equation in X as [7]

$$\rho\frac{\partial^2 U}{\partial t^2} = C_{11}\frac{\partial^2 U}{\partial X^2} + C_{44}\left(\frac{\partial^2 U}{\partial Y^2} + \frac{\partial^2 U}{\partial Z^2}\right) + (C_{12} + C_{44})\left(\frac{\partial^2 U}{\partial X \partial Y} + \frac{\partial^2 U}{\partial X \partial Z}\right), \quad \text{(S5)}$$

where (U, V, W) are in turn the displacements in X, Y, Z directions. Attention is focused on the speeds of shear waves in [100], [110] and [111] directions. By solving

the wave equation, they are $v_{s1}^{[110]} = [(C_{11} - C_{12})/2\rho]^{1/2}$, $v_s^{[111]} = [(C_{11} - C_{12} + C_{44})/3\rho]^{1/2}$ and $v_s^{[100]} = v_{s2}^{[110]} = (C_{44}/\rho)^{1/2}$, respectively. The shear wave in [110] direction has two speeds due to lattice asymmetry. With $C_{11} = 16.84, C_{12} = 12.14, C_{44} = 7.54$ $(10^{10}\mathrm{N/m^3})$ and $\rho = 8900\mathrm{kg/m^3}$ for Cu, one obtains three shear wave speeds, $v_{s1}^{[110]} = 1.63\mathrm{km/s}$, $v_s^{[111]} = 2.16\mathrm{km/s}$ and $v_s^{[100]} = v_{s2}^{[110]} = 2.92\mathrm{km/s}$.

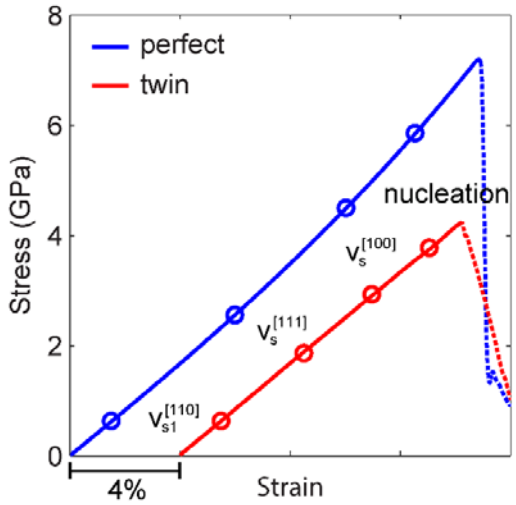

Figure S4. Shear stress-strain curves of the perfect crystal (blue) and the crystal with twin boundaries (red). Critical stress points for $v = v_{s1}^{[110]}$, $v = v_s^{[111]}$, $v = v_s^{[100]}$ and dislocation nucleation are keyed. Here we only show σ_{yz} of the samples under the strain of ε_{yz}.

Note 5: The screw partial in a twin plane

Twinning is another major mechanism to induce plastic deformation in a crystalline solid. The mobility of dislocations on the twin boundary will significantly affect the plasticity of materials. At twin boundary (TB), a full screw dislocation will be separated into two partials, these partials are composed by screw component and edge component, as seen in Fig. S1c and Fig. 1l-m. Their Burgers vectors are $b/2$

for each TSPD, the illustrated stress fields are caused by both edge part and screw part.

Under shearing ε_{yz}, twining partials glide along x-direction in x-z plane. As shown in Fig. 2b, the dislocation moves similarly to that simulated in Fig. 2a, but with a lower critical strain (~9%) for nucleation. Supersonic motion is also observed. We show the velocity field v induced by a moving TSPD in Fig. S5. Typical velocity regions are chosen for illustration. When the dislocation moves supersonically, a Mach cone induced by the screw dislocation appears. Corresponding steady motion at the shear wave velocity for the TSPD are shown in Fig. S6.

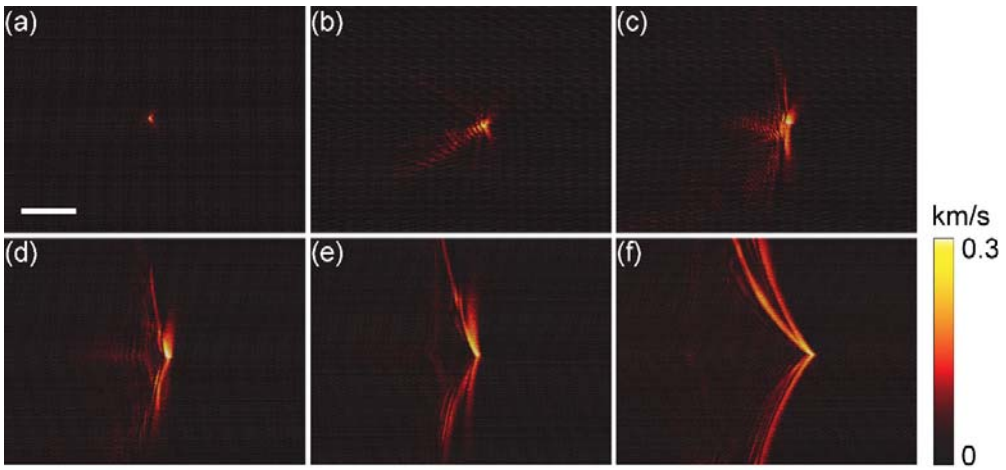

Figure S5. Snapshots of atomic velocity field v induced by the moving TSPD at different velocities. (a) Fast accelerating region at $v = 0.8\,\mathrm{km/s}$; (b) slow acceleration at $v = 1.8\,\mathrm{km/s}$; (c) transient region, $v = v_s^{[111]} = 2.16\,\mathrm{km/s}$; (d) transonic region, $v = 2.5\,\mathrm{km/s}$; (e) transient region $v = v_s^{[100]} = 2.92\,\mathrm{km/s}$; (f) supersonic motion, $v = 3.5\,\mathrm{km/s}$. Emission of shock waves induced by the TSPD is clearly seen. (Scale bar=8 nm).

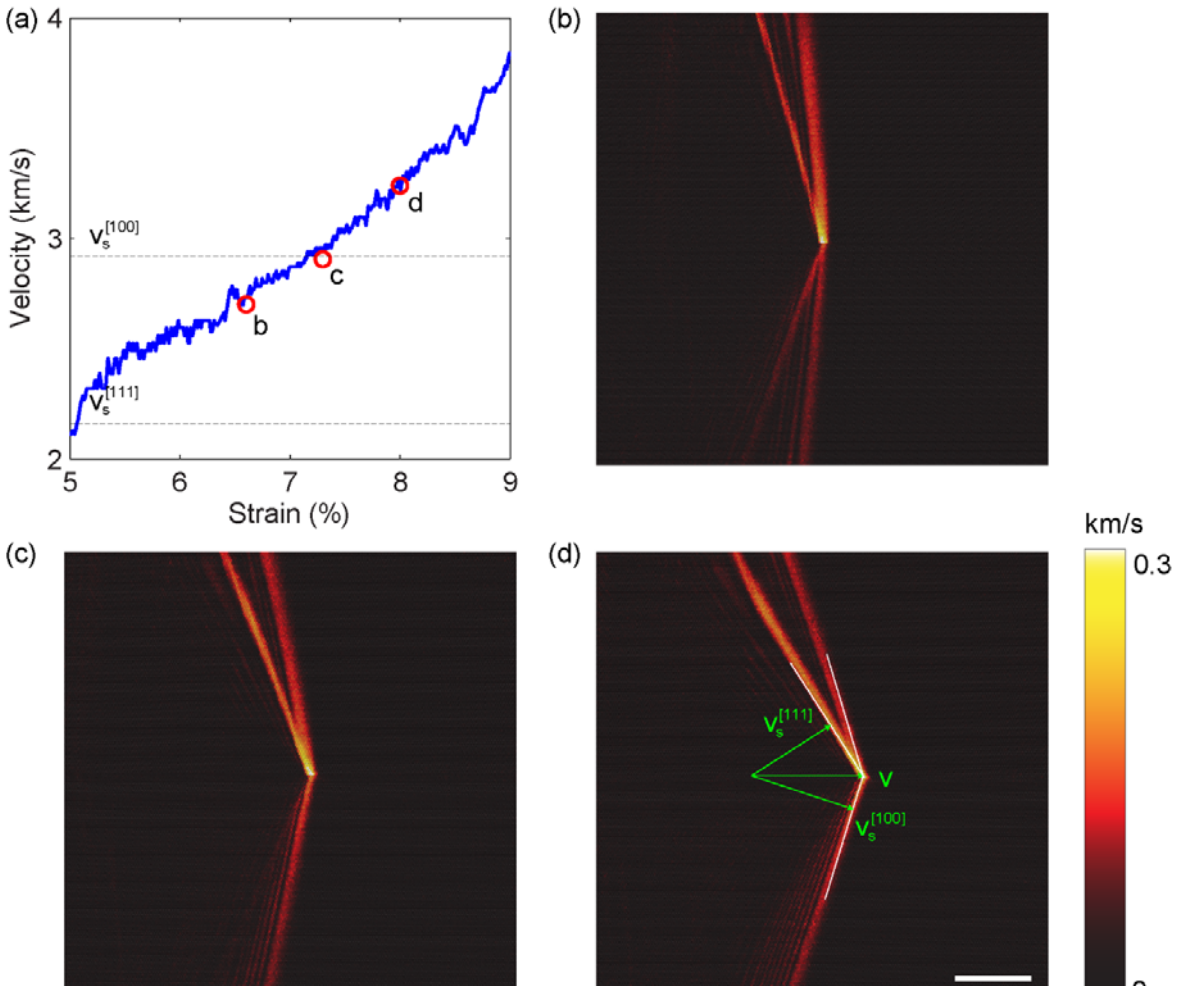

Figure S6. A TSPD moves at the shear wave speed $v_s^{[100]}$. (a) The blue line is the amplified velocity-strain curve from Fig. 2b. Three red circles mark the velocities at which the dislocation could glide steadily. (b)-(d) velocity fields v induced by steadily moving dislocation at three velocities keyed in (a), respectively. (Scale bar=8 nm).

References

[1] S. Plimpton, J. Comput. Phys. 117, 1 (1995).

[2] Y. Mishin, M. J. Mehl, D. A. Papaconstantopoulos, A. F. Voter, and J. D. Kress, Phys. Rev. B 63, 224106 (2001).

[3] D. Faken and H. Jónsson, Comput. Mater. Sci. 2, 279 (1994).

[4] R. Peierls, Proc. Phys. Soc. London 52, 34 (1940).

[5] P. M. Anderson, J. P. Hirth, and J. Lothe, *Theory of Dislocations*, 3rd ed. (Cambridge University Press, Cambridge, England, 2017).

[6] J. D. Eshelby, W. T. Read, and W. Shockley, Acta Metall. 1, 251 (1953).

[7] C. Kittel, Introduction to Solid State Physics, 8th ed. (Wiley, Hoboken, 2005).